Temporal modulation of second harmonic generation in ferroelectrics by a pulsed electric field

Atsushi Ono
Department of Physics, Graduate School of Science, Tohoku University, Sendai 980-8578, Japan

(Received 24 June 2025; revised 15 August 2025; accepted 9 September 2025; published 25 September 2025)

We revisit the relationship between electric polarization modulation ΔP in ferroelectrics induced by a low-frequency pulsed electric field and the corresponding second harmonic intensity modulation $\Delta I_{\rm SH}$. Using nonlinear response theory, we derive their time-domain expressions linear in the pulse amplitude, revealing that not only the electric field but also its time derivative contributes to $\Delta I_{\rm SH}$. Furthermore, even when the time-derivative component is negligible, $\Delta I_{\rm SH}$ can be in antiphase with the pulsed field and thus with ΔP. These theoretical predictions are further supported by real-time simulations of a model for electronic ferroelectrics. Our results demonstrate that the commonly assumed relation $\Delta P \propto \Delta I_{\rm SH}$ can break down under certain conditions, reflecting the complex-valued and frequency-dependent nature of nonlinear dynamical susceptibilities.

DOI: 10.1103/xsrf-t1hj

I. INTRODUCTION

Second harmonic generation (SHG) emerged almost simultaneously with the invention of the laser, when Franken *et al.* observed light at twice the frequency of a ruby laser beam transmitted through quartz [1]. A year later, the perturbation formalism and phase-matching rules were rigorously formulated [2], establishing SHG as a second-order optical process that is forbidden in centrosymmetric crystals and thus sensitive to inversion symmetry breaking [3–7]. Since then, SHG has evolved into a nondestructive probe of ferroelectricity and ferroelectric domains [8–15]; a symmetry probe for multiferroics [16–22] and magnets [23–33]; a valley-selective spectroscopic tool in two-dimensional semiconductors [34–37]; and a probe of quantum geometry [38–51].

More recently, the advent of intense femtosecond and terahertz pulses has broadened interest from static to dynamic symmetry control. Combined with optical pulse excitation, time-resolved SHG spectroscopy enables a direct readout of transient ferroelectric order in quantum paraelectrics [52–57] and ferroelectrics [58–74], as well as other ferroic orders in magnets and multiferroics [75–77]. This technique also probes inversion symmetry breaking in diverse nonequilibrium systems [78–88]. In the quest for dynamic control of symmetry and order in condensed matter, SHG now plays an increasingly pivotal role.

To analyze SHG signals, the following phenomenological expression has been widely used not only under equilibrium conditions but also in nonequilibrium photoexcited states:

$$P_i(2\omega) = \sum_{jk} \tilde{\chi}^{(2)}_{ijk}(2\omega;\omega,\omega) E_j(\omega) E_k(\omega). \tag{1}$$

Here, $E_i(\omega)$ and $P_i(2\omega)$ denote the i-component of the probe electric field at frequency ω and the induced polarization at frequency 2ω, respectively, and $\tilde{\chi}^{(2)}_{ijk}$ is the second-order susceptibility tensor. The intensity of SHG is proportional to the square of $P_i(2\omega)$. The term "phenomenological" is used here because $\tilde{\chi}^{(2)}_{ijk}$ coincides with the microscopic response function derived from time-dependent perturbation theory only when the probe electric field is strictly monochromatic (i.e., a continuous wave).

Even when the probe is approximately monochromatic, additional approximations are often made in discussing the polarization modulation ΔP induced by a pump pulse $E_{\rm pump}$ (indices omitted for simplicity). It is commonly assumed that the second-order susceptibility changes as $\tilde{\chi}^{(2)} \to \tilde{\chi}^{(2)} + \Delta\tilde{\chi}^{(2)}$, with $\Delta\tilde{\chi}^{(2)} \propto E_{\rm pump}$, and hence that the resulting change in the second harmonic intensity is

$$\Delta I_{\rm SH} \propto [\tilde{\chi}^{(2)} + \Delta\tilde{\chi}^{(2)}]^2 - [\tilde{\chi}^{(2)}]^2 \approx 2\tilde{\chi}^{(2)}\Delta\tilde{\chi}^{(2)} \propto E_{\rm pump}. \tag{2}$$

Since $\Delta P \propto E_{\rm pump}$, one then infers that $\Delta P \propto \Delta I_{\rm SH}$. However, $\Delta\tilde{\chi}^{(2)}$ should, in principle, be evaluated as a convolution of the third-order susceptibility with the full spectra of the probe and pump fields [see Eq. (15)], so it is not obvious that $\Delta\tilde{\chi}^{(2)}$ remains strictly in phase with $E_{\rm pump}$. This subtlety appears to have received little attention in the literature, except for a pioneering study by Timm and Bennemann [89].

In this paper, we revisit SHG that is temporally modulated by a pulsed electric field whose frequency is much lower than the probe frequency. In Sec. II, we derive a general expression for $\Delta I_{\rm SH}$ based on microscopic nonlinear response theory. In Sec. III, we validate this expression using real-time simulations of a model ferroelectric system and demonstrate cases in which the relation $\Delta P \propto \Delta I_{\rm SH}$ fails. Sections IV and V provide the discussion and summary, respectively. In Appendix, we present the spectral representation of the nonlinear susceptibility used for a quantitative comparison between theory and simulation.

Published by the American Physical Society under the terms of the Creative Commons Attribution 4.0 International license. Further distribution of this work must maintain attribution to the author(s) and the published article's title, journal citation, and DOI.

II. GENERAL CONSIDERATIONS

We consider the Hamiltonian

$$\mathcal{H}(t) = \mathcal{H}_0 + \mathcal{V}(t), \tag{3}$$

where t is time, $\mathcal{H}_0$ is the unperturbed Hamiltonian, and $\mathcal{V}(t)$ is the time-dependent perturbation:

$$\mathcal{V}(t) = -E(t)P, \tag{4}$$

with $E(t)$ the external electric field and P the electric polarization operator. The expectation value of the electric polarization is given by

$$\langle P\rangle(t) = \mathrm{Tr}[\rho(t)P], \tag{5}$$

where $\rho(t)$ is the density matrix of the system.

According to time-dependent perturbation theory, the nth-order response of the polarization to the electric field is expressed as

$$\langle P\rangle^{(n)}(t) = \int_{-\infty}^{\infty} \mathrm{d}t_1 \cdots \mathrm{d}t_n \, \chi^{(n)}(t; t_1, \ldots, t_n) E(t_1) \cdots E(t_n). \tag{6}$$

Here, the nth-order susceptibility $\chi^{(n)}$ is defined by

$$\begin{aligned}\chi^{(n)}&(t; t_1, t_2, \ldots, t_n) \\ &= \mathrm{i}^n \Theta(t - t_1)\Theta(t_1 - t_2) \cdots \Theta(t_{n-1} - t_n) \\ &\quad \times \langle [[\cdots [[\hat{P}(t), \hat{P}(t_1)], \hat{P}(t_2)], \cdots], \hat{P}(t_n)]\rangle_0,\end{aligned} \tag{7}$$

where $\langle \bullet \rangle_0 = \mathrm{Tr}[\rho(-\infty)\bullet]$ is the expectation value in the initial state, Θ is the unit step function, and $\hat{P}$ is the interaction-picture operator defined by

$$\hat{P}(t) = \mathcal{U}_0(t, -\infty)^\dagger P \mathcal{U}_0(t, -\infty), \tag{8}$$

$$\mathcal{U}_0(t, -\infty) = \mathcal{T} \exp\left(-\mathrm{i}\int_{-\infty}^{t} \mathcal{H}_0 \, \mathrm{d}t'\right), \tag{9}$$

with $\mathcal{T}$ the time-ordering operator. Throughout this paper, we set the Dirac constant $\hbar = 1$. Since Eq. (7) is invariant under time translation,

$$\chi^{(n)}(t; t_1, \ldots, t_n) = \chi^{(n)}(t + T; t_1 + T, \ldots, t_n + T) \tag{10}$$

for any T, we introduce an n-variable susceptibility:

$$\chi^{(n)}(\bar{t}_1, \ldots, \bar{t}_n) = \chi^{(n)}(0; -\bar{t}_1, \ldots, -\bar{t}_n), \tag{11}$$

where $\bar{t}_i = t - t_i$ for $i = 1$ to n. The nth-order susceptibility in the frequency domain is given by

$$\begin{aligned}\chi^{(n)}&(\omega_1, \ldots, \omega_n) \\ &= \int_{-\infty}^{\infty} \mathrm{d}\bar{t}_1 \cdots \mathrm{d}\bar{t}_n \, \mathrm{e}^{\mathrm{i}\omega_1^+ \bar{t}_1} \cdots \mathrm{e}^{\mathrm{i}\omega_n^+ \bar{t}_n} \chi^{(n)}(\bar{t}_1, \ldots, \bar{t}_n),\end{aligned} \tag{12}$$

with $\omega_i^+ = \omega_i + \mathrm{i}\eta$, where $\eta > 0$ is a broadening factor. Since $\hat{P}$ is Hermitian, $\chi^{(n)}$ in Eq. (12) satisfies the relation

$$\chi^{(n)}(\omega_1, \ldots, \omega_n) = \chi^{(n)}(-\omega_1, \ldots, -\omega_n)^*. \tag{13}$$

The Fourier transformation of $\langle P\rangle^{(n)}(t)$ yields

$$\langle P\rangle^{(n)}(\omega) = \int_{-\infty}^{\infty} \mathrm{d}t \, \mathrm{e}^{\mathrm{i}\omega t} \langle P\rangle^{(n)}(t) \tag{14}$$

$$\begin{aligned}&= \int_{-\infty}^{\infty} \frac{\mathrm{d}\omega_1 \cdots \mathrm{d}\omega_n}{(2\pi)^{n-1}} \delta(\omega_1 + \cdots + \omega_n - \omega) \\ &\quad \times \chi^{(n)}(\omega_1, \ldots, \omega_n) E(\omega_1) \cdots E(\omega_n),\end{aligned} \tag{15}$$

where δ represents the delta function. Unlike Eq. (1), Eq. (15) is valid for arbitrary $E(\omega)$.

In what follows, we discuss the temporal modulations in the polarization and the second harmonic (SH) intensity induced by the following external electric field:

$$E(t) = E_{\mathrm{IR}} \cos(\omega_{\mathrm{IR}} t) + E_{\mathrm{THz}}(t), \tag{16}$$

where the first and second terms represent an infrared (IR) probe and a terahertz (THz) pump, respectively. In the frequency domain, the electric field is expressed as

$$E(\omega) = E_{\mathrm{IR}} \pi [\delta(\omega - \omega_{\mathrm{IR}}) + \delta(\omega + \omega_{\mathrm{IR}})] + E_{\mathrm{THz}}(\omega). \tag{17}$$

A. Electric polarization

Setting $E_{\mathrm{IR}} = 0$ and substituting Eq. (17) into Eq. (15), we obtain the well-known expression for the polarization change linear in E_{THz} as follows:

$$\langle P\rangle^{(1)}(\omega) = \chi^{(1)}(\omega) E_{\mathrm{THz}}(\omega). \tag{18}$$

When $E_{\mathrm{THz}}(\omega)$ is sharply peaked around $\omega = 0$, $\chi^{(1)}(\omega)$ can be approximated by its value at $\omega = 0$, yielding

$$\langle P\rangle^{(1)}(\omega) \approx \chi^{(1)}(\omega = 0) E_{\mathrm{THz}}(\omega). \tag{19}$$

Since $\chi^{(1)}(\omega = 0)$ is real-valued, as follows from Eq. (13), there is no phase delay between the polarization and the pulsed field. Accordingly, in the time domain, we arrive at the relation

$$\Delta P(t) \equiv \langle P\rangle^{(1)}(t) \propto E_{\mathrm{THz}}(t). \tag{20}$$

B. Second harmonic generation

We now consider the second-order response of the IR probe under the THz pump pulse described by Eq. (16). For the response in the absence of the pump pulse, by substituting Eq. (17) into Eq. (15) and extracting the dominant contributions near $\omega = \pm 2\omega_{\mathrm{IR}}$, we obtain

$$\begin{aligned}P^{(2)}(\omega) &= \frac{\pi}{4} \bar{\chi}^{(2)}(\omega_{\mathrm{IR}}, \omega_{\mathrm{IR}}) E_{\mathrm{IR}}^2 \delta(\omega - 2\omega_{\mathrm{IR}}) \\ &\quad + \frac{\pi}{4} \bar{\chi}^{(2)}(-\omega_{\mathrm{IR}}, -\omega_{\mathrm{IR}}) E_{\mathrm{IR}}^2 \delta(\omega + 2\omega_{\mathrm{IR}}).\end{aligned} \tag{21}$$

Similarly, the pump-induced response linear in E_{THz} can be expressed in terms of the third-order susceptibility as

$$\begin{aligned}P^{(3)}(\omega) &= \tfrac{1}{8} \bar{\chi}^{(3)}(\omega_{\mathrm{IR}}, \omega_{\mathrm{IR}}, \omega - 2\omega_{\mathrm{IR}}) E_{\mathrm{IR}}^2 E_{\mathrm{THz}}(\omega - 2\omega_{\mathrm{IR}}) \\ &\quad + \tfrac{1}{8} \bar{\chi}^{(3)}(-\omega_{\mathrm{IR}}, -\omega_{\mathrm{IR}}, \omega + 2\omega_{\mathrm{IR}}) E_{\mathrm{IR}}^2 E_{\mathrm{THz}}(\omega + 2\omega_{\mathrm{IR}}).\end{aligned} \tag{22}$$

In Eqs. (21) and (22), we define the symmetrized susceptibility as

$$\bar{\chi}^{(n)}(\omega_1, \ldots, \omega_n) = \sum_{s \in \mathfrak{S}_n} \chi^{(n)}(\omega_{s(1)}, \ldots, \omega_{s(n)}), \tag{23}$$

where $\mathfrak{S}_n$ represents the symmetric group of degree n.

The far field of the electric dipole radiation, which is proportional to the second derivative of $P(t)$, is defined as follows (up to a multiplicative constant):

$$E_\infty(t) = -\ddot{P}(t), \quad E_\infty(\omega) = \omega^2 P(\omega). \tag{24}$$

By substituting Eq. (17) into Eq. (24), we obtain

$$\begin{aligned} E_\infty(\omega) &= \frac{\pi}{4}E_{\mathrm{IR}}^2[(2\omega_{\mathrm{IR}})^2\bar{\chi}^{(2)}(\omega_{\mathrm{IR}},\omega_{\mathrm{IR}})\delta(\omega-2\omega_{\mathrm{IR}}) \\ &\quad + (-2\omega_{\mathrm{IR}})^2\bar{\chi}^{(2)}(-\omega_{\mathrm{IR}},-\omega_{\mathrm{IR}})\delta(\omega+2\omega_{\mathrm{IR}})] \\ &\quad + \frac{1}{8}E_{\mathrm{IR}}^2[\omega^2\bar{\chi}^{(3)}(\omega_{\mathrm{IR}},\omega_{\mathrm{IR}},\omega-2\omega_{\mathrm{IR}})E_{\mathrm{THz}}(\omega-2\omega_{\mathrm{IR}}) \\ &\quad + \omega^2\bar{\chi}^{(3)}(-\omega_{\mathrm{IR}},-\omega_{\mathrm{IR}},\omega+2\omega_{\mathrm{IR}})E_{\mathrm{THz}}(\omega+2\omega_{\mathrm{IR}})]. \end{aligned} \tag{25}$$

To simplify notation, we introduce the following shorthand:

$$\bar{\chi}_2 = \bar{\chi}^{(2)}(\omega_{\mathrm{IR}},\omega_{\mathrm{IR}}), \tag{26}$$

$$\bar{\chi}_3 = \bar{\chi}^{(3)}(\omega_{\mathrm{IR}},\omega_{\mathrm{IR}},0), \tag{27}$$

$$\bar{\chi}_3' = \left.\frac{\partial\bar{\chi}^{(3)}(\omega_{\mathrm{IR}},\omega_{\mathrm{IR}},\omega-2\omega_{\mathrm{IR}})}{\partial\omega}\right|_{\omega=2\omega_{\mathrm{IR}}}. \tag{28}$$

The third-order susceptibility is then expanded around $\omega = \pm 2\omega_{\mathrm{IR}}$ as

$$\bar{\chi}^{(3)}(\omega_{\mathrm{IR}},\omega_{\mathrm{IR}},\omega-2\omega_{\mathrm{IR}}) \approx \bar{\chi}_3 + (\omega-2\omega_{\mathrm{IR}})\bar{\chi}_3', \tag{29}$$

$$\begin{aligned} \bar{\chi}^{(3)}(-\omega_{\mathrm{IR}},-\omega_{\mathrm{IR}},\omega+2\omega_{\mathrm{IR}}) &= \bar{\chi}^{(3)}(\omega_{\mathrm{IR}},\omega_{\mathrm{IR}},-\omega-2\omega_{\mathrm{IR}})^* \\ &\approx \bar{\chi}_3^* - (\omega+2\omega_{\mathrm{IR}})\bar{\chi}_3'^*, \end{aligned} \tag{30}$$

where we have used Eq. (13). By performing the inverse Fourier transformation of $E_\infty(\omega)$ and neglecting second- and higher-order derivatives of $E_{\mathrm{THz}}(t)$, we obtain the time-domain expression for the far field:

$$\begin{aligned} E_\infty(t) &= \left\{\omega_{\mathrm{IR}}^2|\bar{\chi}_2|\cos(\phi_2) + \omega_{\mathrm{IR}}^2|\bar{\chi}_3|\cos(\phi_3)E_{\mathrm{THz}}(t) - \left[\omega_{\mathrm{IR}}|\bar{\chi}_3|\sin(\phi_3) + \omega_{\mathrm{IR}}^2|\bar{\chi}_3'|\sin(\phi_3')\right]\dot{E}_{\mathrm{THz}}(t)\right\}E_{\mathrm{IR}}^2\cos(2\omega_{\mathrm{IR}}t) \\ &\quad + \left\{\omega_{\mathrm{IR}}^2|\bar{\chi}_2|\sin(\phi_2) + \omega_{\mathrm{IR}}^2|\bar{\chi}_3|\sin(\phi_3)E_{\mathrm{THz}}(t) + \left[\omega_{\mathrm{IR}}|\bar{\chi}_3|\cos(\phi_3) + \omega_{\mathrm{IR}}^2|\bar{\chi}_3'|\cos(\phi_3')\right]\dot{E}_{\mathrm{THz}}(t)\right\}E_{\mathrm{IR}}^2\sin(2\omega_{\mathrm{IR}}t), \end{aligned} \tag{31}$$

where $\phi_2 = \arg\bar{\chi}_2$, $\phi_3 = \arg\bar{\chi}_3$, and $\phi_3' = \arg\bar{\chi}_3'$.

The appearance of the time derivative of $E_{\mathrm{THz}}(t)$ in Eq. (31) can be attributed to two distinct origins. The first arises from the fact that the far field $E_\infty(t)$ is proportional to the second derivative of the polarization, as shown in Eq. (24). Specifically, the term $\omega^2 E_{\mathrm{THz}}(\omega\mp 2\omega_{\mathrm{IR}})$ in Eq. (25) leads to time derivatives of $E_{\mathrm{THz}}(t)$ through its inverse Fourier transformation:

$$\begin{aligned} &\int_{-\infty}^{\infty}\frac{\mathrm{d}\omega}{2\pi}\mathrm{e}^{-\mathrm{i}\omega t}\omega^2 E_{\mathrm{THz}}(\omega\mp 2\omega_{\mathrm{IR}}) \\ &= -\frac{\mathrm{d}^2}{\mathrm{d}t^2}\int_{-\infty}^{\infty}\frac{\mathrm{d}\omega}{2\pi}\mathrm{e}^{-\mathrm{i}\omega t}\int_{-\infty}^{\infty}\mathrm{d}t'\mathrm{e}^{\mathrm{i}(\omega\mp 2\omega_{\mathrm{IR}})t'}E_{\mathrm{THz}}(t') \\ &= \mathrm{e}^{\mp 2\mathrm{i}\omega_{\mathrm{IR}}t}\left[4\omega_{\mathrm{IR}}^2 E_{\mathrm{THz}}(t) \pm 4\mathrm{i}\omega_{\mathrm{IR}}\dot{E}_{\mathrm{THz}}(t) - \ddot{E}_{\mathrm{THz}}(t)\right]. \end{aligned} \tag{32}$$

The second origin is the frequency dependence of the third-order susceptibility $\bar{\chi}^{(3)}(\pm\omega_{\mathrm{IR}},\pm\omega_{\mathrm{IR}},\omega\mp 2\omega_{\mathrm{IR}})$. When $\chi^{(3)}$ is expanded around $\omega = \pm 2\omega_{\mathrm{IR}}$, as in Eqs. (29) and (30), the linear term in $\omega\mp 2\omega_{\mathrm{IR}}$ produces a contribution proportional to $\dot{E}_{\mathrm{THz}}(t)$ via inverse Fourier transformation:

$$\begin{aligned} &\int_{-\infty}^{\infty}\frac{\mathrm{d}\omega}{2\pi}\mathrm{e}^{-\mathrm{i}\omega t}\omega^2(\omega\mp 2\omega_{\mathrm{IR}})E_{\mathrm{THz}}(\omega\mp 2\omega_{\mathrm{IR}}) \\ &= \mathrm{i}\frac{\mathrm{d}^2}{\mathrm{d}t^2}\int_{-\infty}^{\infty}\frac{\mathrm{d}\omega}{2\pi}\mathrm{e}^{-\mathrm{i}\omega t}\int_{-\infty}^{\infty}\mathrm{d}t'\frac{\mathrm{d}\mathrm{e}^{\mathrm{i}(\omega\mp 2\omega_{\mathrm{IR}})t'}}{\mathrm{d}t'}E_{\mathrm{THz}}(t') \\ &= -\mathrm{i}\frac{\mathrm{d}^2}{\mathrm{d}t^2}\int_{-\infty}^{\infty}\frac{\mathrm{d}\omega}{2\pi}\mathrm{e}^{-\mathrm{i}\omega t}\int_{-\infty}^{\infty}\mathrm{d}t'\mathrm{e}^{\mathrm{i}(\omega\mp 2\omega_{\mathrm{IR}})t'}\dot{E}_{\mathrm{THz}}(t') \\ &= \mathrm{i}\mathrm{e}^{\mp 2\mathrm{i}\omega_{\mathrm{IR}}t}\left[4\omega_{\mathrm{IR}}^2\dot{E}_{\mathrm{THz}}(t) \pm 4\mathrm{i}\omega_{\mathrm{IR}}\ddot{E}_{\mathrm{THz}}(t) - \dddot{E}_{\mathrm{THz}}(t)\right], \end{aligned} \tag{33}$$

which is reflected in the terms involving $\bar{\chi}_3'$ in Eq. (31).

Since Eq. (31) takes the form of $E_\infty(t) = A(t)\cos(2\omega_{\mathrm{IR}}t) + B(t)\sin(2\omega_{\mathrm{IR}}t)$, where $A(t)$ and $B(t)$ are slowly varying functions of time, the SH intensity is given by the time-averaged square of the field: $\overline{E_\infty(t)^2} \approx [A(t)^2 + B(t)^2]/2$. This leads to the following expressions for the SH intensity in equilibrium,

$$I_{\mathrm{SH}} = \tfrac{1}{2}\omega_{\mathrm{IR}}^4|\bar{\chi}_2|^2E_{\mathrm{IR}}^4, \tag{34}$$

and for the temporal modulation of the SH intensity linearly induced by the pulsed field,

$$\begin{aligned} \Delta I_{\mathrm{SH}}(t) = \omega_{\mathrm{IR}}^4|\bar{\chi}_2|E_{\mathrm{IR}}^4\Bigg\{&|\bar{\chi}_3|\cos(\phi_2-\phi_3)E_{\mathrm{THz}}(t) \\ &+ \left[\frac{|\bar{\chi}_3|}{\omega_{\mathrm{IR}}}\sin(\phi_2-\phi_3) + |\bar{\chi}_3'|\sin(\phi_2-\phi_3')\right] \\ &\times\dot{E}_{\mathrm{THz}}(t)\Bigg\}. \end{aligned} \tag{35}$$

Therefore, the relative change in the SH intensity, $\Delta I_{\mathrm{SH}}/I_{\mathrm{SH}}$, can be expressed in the form

$$\frac{\Delta I_{\mathrm{SH}}}{I_{\mathrm{SH}}} = C_0E_{\mathrm{THz}}(t) + C_1\frac{\dot{E}_{\mathrm{THz}}(t)}{\omega_{\mathrm{THz}}}, \tag{36}$$

where the coefficients C_0 and $C_1 \equiv C_{10} + C_{11}$ are given by

$$C_0 = \frac{2|\bar{\chi}_3|}{|\bar{\chi}_2|}\cos(\phi_2-\phi_3), \tag{37}$$

$$C_{10} = \frac{2\omega_{\mathrm{THz}}|\bar{\chi}_3|}{\omega_{\mathrm{IR}}|\bar{\chi}_2|}\sin(\phi_2-\phi_3), \tag{38}$$

$$C_{11} = \frac{2\omega_{\mathrm{THz}}|\bar{\chi}_3'|}{|\bar{\chi}_2|}\sin(\phi_2-\phi_3'). \tag{39}$$

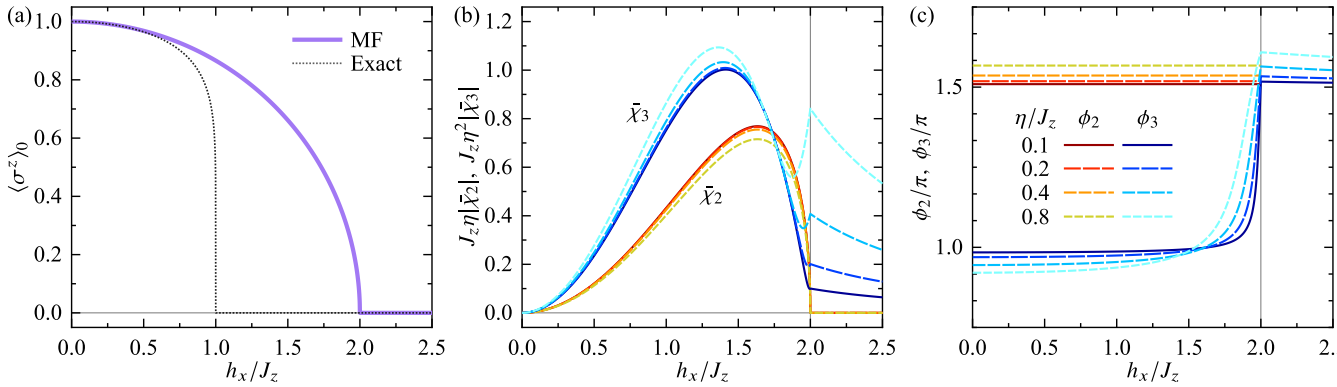


FIG. 1. (a) Electric polarization $\langle\sigma^z\rangle_0$ in the ground state. The dotted curve indicates the exact result, $[1-(h_x/J_z)^2]^{1/8}$. (b) Absolute values and (c) phases of $\bar{\chi}_2$ and $\bar{\chi}_3$ for $\eta/J_z = 0.1$ (solid) to 0.8 (dashed) and $\omega_{\rm IR} = E_{\rm g}/2$. The phase ϕ_2 is undefined for $h_x/J_z \geqslant 2$.

A notable result is that, unlike the polarization change $\Delta P(t)$ in Eq. (20), the SH intensity change $\Delta I_{\rm SH}(t)$ depends not only on $E_{\rm THz}(t)$ but also on its time derivative $\dot{E}_{\rm THz}(t)$. Furthermore, even if the time-derivative component C_1 is negligible, the sign of C_0 can be negative; that is, $\Delta I_{\rm SH}(t)$ can be in antiphase with $E_{\rm THz}(t)$. Consequently, the commonly assumed relation $\Delta P(t) \propto \Delta I_{\rm SH}(t)$ does not generally hold.

III. NUMERICAL ANALYSIS

In this section, we consider a concrete model for ferroelectrics to quantitatively evaluate the contribution of $\dot{E}_{\rm THz}(t)$ to $\Delta I_{\rm SH}$. We introduce the model in Sec. III A, followed by an evaluation of its second- and third-order susceptibilities using the spectral representations in Sec. III B. The real-time simulation method is detailed in Sec. III C. We then show the numerical results in Sec. III D to verify the theoretical prediction provided by Eq. (35).

A. Model

We consider the one-dimensional Ising model with a transverse field, whose Hamiltonian is given by

$$\mathcal{H}_0 = -J_z \sum_i \sigma_i^z \sigma_{i+1}^z - h_x \sum_i \sigma_i^x, \tag{40}$$

where σ_i^α $(\alpha = x, y, z)$ denotes the Pauli matrix at site i. This spin model captures the essential features of electronic ferroelectricity [90,91]: the Ising interaction J_z stabilizes the ferroelectric phase with $\langle\sigma_i^z\rangle_0 \neq 0$, while the transverse field h_x favors the quantum paraelectric phase with $\langle\sigma_i^z\rangle_0 = 0$ [92,93]. Hereafter, we employ the mean-field (MF) approximation to make the problem tractable, which also enables us to derive explicit expressions for the nonlinear susceptibilities. The MF Hamiltonian is given by

$$\mathcal{H}_0^{\rm MF} = -h_z\sigma^z - h_x\sigma^x, \quad h_z = 2J_z s_z, \tag{41}$$

where the order parameter $s_z = \langle\sigma^z\rangle_0$ is the electric polarization, and the site index has been omitted. The MF Hamiltonian is diagonalized by a unitary transformation $U_y(\theta)^\dagger \mathcal{H}_0^{\rm MF} U_y(\theta)$ with $U_y(\theta) = \exp(-{\rm i}\theta\sigma^y/2)$ and $\theta = \arctan(h_x/h_z)$, yielding

$$U_y(\theta)^\dagger \mathcal{H}_0^{\rm MF} U_y(\theta) = \begin{bmatrix} \varepsilon_- & 0 \\ 0 & \varepsilon_+ \end{bmatrix}, \quad \varepsilon_\pm = \pm\sqrt{h_z^2 + h_x^2}. \tag{42}$$

The ground state and excited state are given by $|0\rangle = U_y(\theta)|\uparrow\rangle$ and $|1\rangle = U_y(\theta)|\downarrow\rangle$, respectively, where $|\uparrow\rangle$ and $|\downarrow\rangle$ are the eigenstates of σ^z satisfying $\sigma^z|\uparrow\rangle = |\uparrow\rangle$ and $\sigma^z|\downarrow\rangle = -|\downarrow\rangle$.

The order parameter s_z is determined by the self-consistent equation

$$s_z = \langle\sigma^z\rangle_0 = \frac{2J_z s_z}{\sqrt{4J_z^2 s_z^2 + h_x^2}} \tag{43}$$

at zero temperature. The solution of Eq. (43) is

$$s_z = \begin{cases} \sqrt{4J_z^2 - h_x^2}\,\Big/(2J_z) & (2J_z > h_x > 0) \\ 0 & (h_x > 2J_z > 0), \end{cases} \tag{44}$$

which is plotted in Fig. 1(a), along with the exact solution [94] for reference. The ground state is ferroelectric for $h_x/J_z < 2$ and paraelectric for $h_x/J_z > 2$. The energy gap between $|0\rangle$ and $|1\rangle$ can be expressed as

$$E_{\rm g} = \varepsilon_+ - \varepsilon_- = \begin{cases} 4J_z & (2J_z > h_x > 0) \\ 2h_x & (h_x > 2J_z > 0). \end{cases} \tag{45}$$

The matrix elements of the polarization operator $P = \sigma^z$ are

$$\langle 0|P|0\rangle = -\langle 1|P|1\rangle = \langle\sigma^z\rangle_0, \tag{46}$$

$$\langle 0|P|1\rangle = \begin{cases} -h_x/(2J_z) & (2J_z > h_x > 0) \\ -1 & (h_x > 2J_z > 0). \end{cases} \tag{47}$$

B. Nonlinear susceptibility

Here, we present the explicit forms of the second- and third-order susceptibilities in the ferroelectric ground state, using their spectral representation presented in Appendix. Assuming that $2\omega_{\rm IR}$ is resonant with the energy gap $E_{\rm g} = 4J_z$, and substituting Eqs. (44)–(47) into the spectral representation, we obtain the expression for $\bar{\chi}_2$ in Eq. (26) as

$$\bar{\chi}_2 = \frac{32h_x^2(3J_z + {\rm i}\eta)\sqrt{4J_z^2 - h_x^2}}{{\rm i}\eta J_z(2J_z - {\rm i}\eta)(4J_z + {\rm i}\eta)(6J_z + {\rm i}\eta)(8J_z + {\rm i}\eta)}, \tag{48}$$

where η is a broadening factor. This is plotted in Figs. 1(b) and 1(c) for $\eta/J_z = 0.1$, 0.2, 0.4, and 0.8 (solid to dashed lines). As $\eta \to 0$, Eq. (48) asymptotically reduces to

$$\bar{\chi}_2 \to h_x^2\sqrt{4J_z^2 - h_x^2}\left(\frac{7}{96J_z^5} - {\rm i}\frac{1}{4J_z^4\eta}\right) + \mathcal{O}(\eta^1), \tag{49}$$

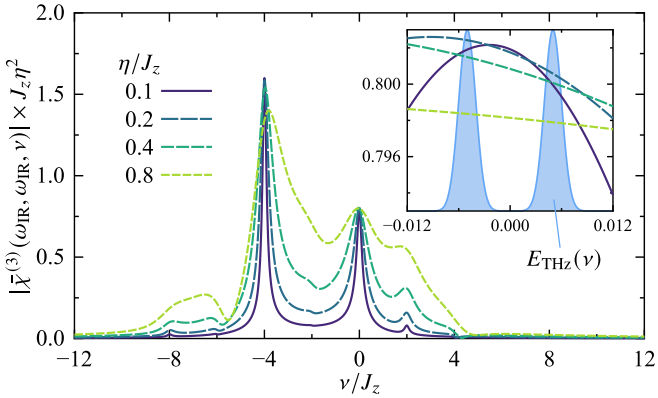


FIG. 2. Third-order susceptibility $\bar{\chi}^{(3)}(\omega_{\rm IR},\omega_{\rm IR},\nu=\omega-2\omega_{\rm IR})$ for $\eta/J_z=0.1$ to 0.8, with $h_x/J_z=1.7$ and $\omega_{\rm IR}=E_{\rm g}/2$. The inset provides an enlarged view, where the shaded blue curve represents $E_{\rm THz}(\nu)$.

and thus $|\bar{\chi}_2|$ scales as η^{-1}, as shown in Fig. 1(b). Note that, near the transition point $h_x/J_z=2$, the polarization $\langle\sigma^z\rangle_0$ is proportional to $|\bar{\chi}_2|$, whereas this relation fails for $h_x/J_z\lesssim 1.8$. This is because the magnitude of the transition dipole moment in Eq. (47) decreases as h_x decreases.

For the third-order susceptibility, since the full forms of $\bar{\chi}_3$ and $\bar{\chi}_3'$ in Eqs. (27) and (28) are cumbersome, we present their asymptotic expressions:

$$\bar{\chi}_3\to-\frac{4J_z^2h_x^2-h_x^4}{4J_z^5\eta^2}+\mathrm{i}\frac{8J_z^2h_x^2-3h_x^4}{16J_z^6\eta}+\mathcal{O}(\eta^0), \tag{50}$$

$$\bar{\chi}_3'\to-\frac{2J_z^2h_x^2-h_x^4}{8J_z^6\eta^2}-\mathrm{i}\frac{4J_z^2h_x^2-h_x^4}{4J_z^5\eta^3}+\mathcal{O}(\eta^{-1}). \tag{51}$$

The exact absolute value and phase of $\bar{\chi}_3$ for $\eta/J_z=0.1$–0.8 are also shown in Figs. 1(b) and 1(c), which are well approximated by the asymptotic expressions (not shown). In the ferroelectric phase, $|\bar{\chi}_3|$ scales as η^{-2} [see Eq. (50)], while in the paraelectric phase it scales as η^{-1}. Additionally, the frequency dependence of $\bar{\chi}^{(3)}(\omega_{\rm IR},\omega_{\rm IR},\nu)$ in Eq. (25) is plotted in Fig. 2, showing a resonance peak at $\nu=0$. From Eqs. (49)–(51), the coefficients in Eqs. (37)–(39) can be evaluated as follows:

$$C_0\to\frac{25h_x^2-76J_z^2}{12J_z^2\sqrt{4J_z^2-h_x^2}}+\mathcal{O}(\eta^2), \tag{52}$$

$$C_{10}\to\frac{2\sqrt{4J_z^2-h_x^2}}{J_z}\frac{\omega_{\rm THz}}{\omega_{\rm IR}\eta}+\mathcal{O}(\eta^1), \tag{53}$$

$$C_{11}\to\frac{52J_z^2-19h_x^2}{12J_z^2\sqrt{4J_z^2-h_x^2}}\frac{\omega_{\rm THz}}{\eta}+\mathcal{O}(\eta^1). \tag{54}$$

The coefficient C_0 vanishes and changes sign at $h_x/J_z=\sqrt{76/25}\approx 1.74$, around which the time-derivative component proportional to C_1 is expected to dominate. This prediction will be numerically verified in Sec. III D.

C. Real-time simulation

To validate the theoretical predictions presented in Sec. II, we perform real-time simulations of the MF model in Eq. (41) when a terahertz pulse is applied. Here, we describe the methodological details.

The density matrix $\rho(t)$ evolves according to the von Neumann equation with a relaxation-time approximation:

$$\dot{\rho}(t)=-\mathrm{i}[\mathcal{H}(t),\rho(t)]-\Gamma[\rho(t)-\rho_0], \tag{55}$$

where Γ is the relaxation rate, and $\rho_0=|0\rangle\langle 0|$ represents the density matrix of the ground state. The time-dependent Hamiltonian is given by

$$\mathcal{H}(t)=-h_z(t)\sigma^z-h_x\sigma^x, \tag{56}$$

$$h_z(t)=2J_z\langle\sigma^z\rangle_0+E(t), \tag{57}$$

where $E(t)$ is the total electric field from Eq. (16), comprising a continuous wave (IR probe) and an off-resonant terahertz pump pulse:

$$E(t)=E_{\rm IR}\cos(\omega_{\rm IR}t)+E_{\rm THz}(t), \tag{58}$$

$$E_{\rm THz}(t)=E_{\rm THz}^0\exp\left(-\frac{t^2}{2t_{\rm w}^2}\right)\cos(\omega_{\rm THz}t). \tag{59}$$

Hereafter, we set $E_{\rm IR}=0.005J_z$, $\omega_{\rm IR}=E_{\rm g}/2=2J_z$, $E_{\rm THz}^0=10^{-5}J_z$, $\omega_{\rm THz}=0.005J_z$, and $t_{\rm w}=1000J_z^{-1}$. The Fourier spectrum of the terahertz pulse is shown in the inset of Fig. 2, along with $\bar{\chi}^{(3)}(\omega_{\rm IR},\omega_{\rm IR},\nu)$ for various η. For the parameters adopted, we observe that $\bar{\chi}^{(3)}(\omega_{\rm IR},\omega_{\rm IR},\nu)$ remains nearly constant over the spectral range of $E_{\rm THz}(\nu)$, which justifies the linear approximation employed in Eqs. (29) and (30). In the simulations presented in Sec. III D, we focus on the case with $\Gamma=\eta=0.1J_z$, which corresponds to the worst-case scenario for the linear approximation accuracy among the η values shown in Fig. 2.

To evaluate the SH response, we first compute the second derivative of the polarization,

$$\ddot{s}_z(t)=\mathrm{Tr}[\ddot{\rho}(t)\sigma^z], \tag{60}$$

where $\ddot{\rho}(t)$ is explicitly obtained by differentiating Eq. (55):

$$\ddot{\rho}(t)=-\mathrm{i}[\dot{\mathcal{H}}(t),\rho(t)]-\mathrm{i}[\mathcal{H}(t),\dot{\rho}(t)]-\Gamma\dot{\rho}(t), \tag{61}$$

$$\dot{\mathcal{H}}(t)=-\dot{E}(t)\sigma^z. \tag{62}$$

Figure 3(a) shows an example of the temporal profile of $\ddot{s}_z(t)$. Since $E_{\rm IR}\gg E_{\rm THz}^0$, a sinusoidal oscillation at the probe frequency $\omega_{\rm IR}$ is predominantly observed. We then extract the SH amplitude by applying a windowed Fourier transformation to $\ddot{s}_z(t)$. Specifically, we slide a time window of width $T=2\pi M/\omega_{\rm IR}$, where M is an integer, and then compute the discrete Fourier transformation:

$$\mathrm{FT}[\ddot{s}](\omega,t)=\frac{2\Delta t}{T}\mathrm{e}^{\mathrm{i}\omega(t-T/2)}\sum_{n=0}^{\frac{T}{\Delta t}-1}\mathrm{e}^{\mathrm{i}\omega n\Delta t}\ddot{s}_z(t-T/2+n\Delta t), \tag{63}$$

where Δt is the fixed time step used in the fourth-order Runge–Kutta integration of Eq. (55). To ensure that the frequency grid contains exactly the integer multiples of the probe frequency $\omega_{\rm IR}$, we set

$$\Delta t=\frac{T}{2N_{\rm max}M}, \tag{64}$$

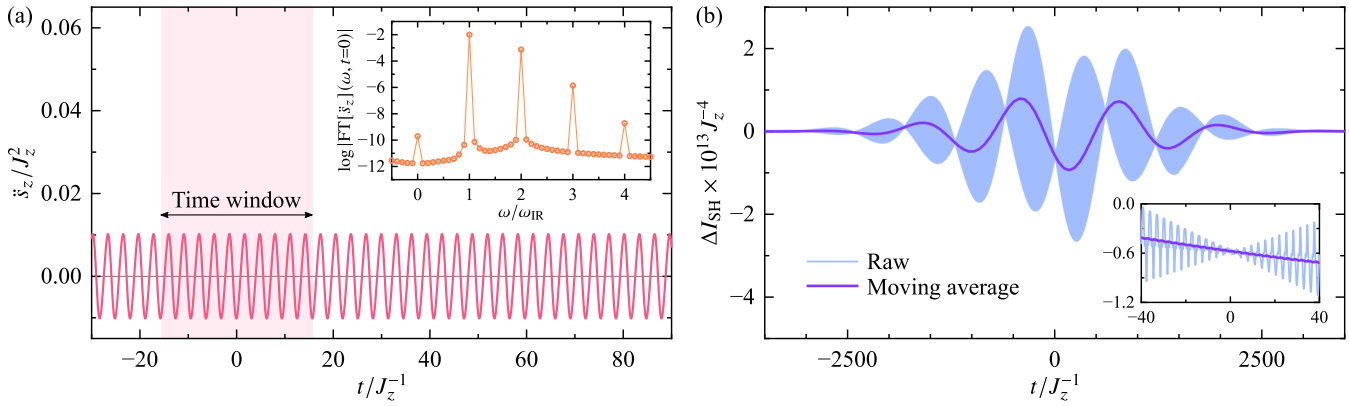


FIG. 3. (a) Second derivative of the polarization, $\ddot{s}_z(t)$. The inset shows its Fourier amplitude within the shaded time window centered at $t = 0$. (b) Change in the SH intensity, $\Delta I_{\mathrm{SH}}(t)$. The inset is an enlarged view around $t = 0$. The blue and the bold purple curves indicate the raw data and the moving-average data, respectively. The transverse field strength is set to $h_x/J_z = 1.74$ in (a) and (b).

with $N_{\max}$ denoting the highest positive harmonic order to be resolved. The prefactor $2\Delta t/T$ in Eq. (63) is chosen such that $|\mathrm{FT}[\ddot{s}](\omega, t)| = A$ when $\ddot{s}_z(t) = A\cos(\omega t)$. In our calculations, we choose $M = 10$ and the smallest integer $N_{\max} = 158$ such that $\Delta t \leqslant 0.01 J_z^{-1}$. This approach based on the discrete Fourier transformation was also adopted in a previous study of high harmonic generation [95].

From the Fourier spectrum in Eq. (63), we extract the SH amplitude at $\omega = 2\omega_{\mathrm{IR}}$ and compute the time-averaged SH intensity as

$$I_{\mathrm{SH}} + \Delta I_{\mathrm{SH}}(t) = \frac{|\mathrm{FT}[\ddot{s}](2\omega_{\mathrm{IR}}, t)|^2}{2}. \tag{65}$$

Since this quantity exhibits rapid oscillations [see the blue curve in Fig. 3(b)], we apply a moving average over a time span of $4\pi/\omega_{\mathrm{IR}}$, thereby obtaining a slowly varying SH intensity [the bold purple curve in Fig. 3(b)] that directly corresponds to Eq. (35).

D. Numerical results

Figure 4 shows the temporal changes in polarization $\Delta P(t)$ and SH intensity $\Delta I_{\mathrm{SH}}(t)$. The temporal profiles of $\Delta P/P$ in Figs. 4(a)–(d) closely follow the waveform of the terahertz pulse, $E_{\mathrm{THz}}(t)$, and their amplitude increases with increasing h_x. By contrast, the changes in the SH intensity are more pronounced. For $h_x/J_z = 1.78$ [Fig. 4(h)], $\Delta I_{\mathrm{SH}}(t)$ is nearly in phase with $E_{\mathrm{THz}}(t)$, whereas for $h_x/J_z = 1.7$ [Fig. 4(e)], it is in antiphase. At intermediate values $h_x/J_z = 1.74$ and 1.745 [Figs. 4(f) and 4(g)], $\Delta I_{\mathrm{SH}}(t)$ exhibits a distinct phase shift relative to $E_{\mathrm{THz}}(t)$. The red lines in Figs. 4(e)–(h) represent the fits to Eq. (36), where C_0 and C_1 are treated as fitting parameters. These results indicate that, in addition to the component proportional to $E_{\mathrm{THz}}(t)$ (dotted blue lines), a significant contribution proportional to $\dot{E}_{\mathrm{THz}}(t)$ (dashed green lines) emerges despite $\omega_{\mathrm{THz}} \ll \omega_{\mathrm{IR}}$, as predicted in Sec. II.

We performed the same fitting procedure for various values of h_x and plotted the ratio of the time-derivative component, C_1/C_0, as a function of h_x in Fig. 5(a). The black circles are simulation results obtained with a relaxation rate of $\Gamma/J_z = 0.1$, while the solid red line represents the analytical prediction from Eqs. (37)–(39) using a broadening factor $\eta/J_z = 0.1$. The two results agree remarkably well, validating our theoretical framework. As expected from the asymptotic analysis in Sec. III B, C_1/C_0 diverges near $h_x/J_z \approx 1.74$. This divergence occurs because C_0 vanishes at $h_x/J_z \approx 1.7427$, as shown in Fig. 5(b). Figure 5(c) plots C_1 along with its components C_{10} and C_{11}. In the region where C_1/C_0 diverges, C_1 remains nonzero, and contributions from C_{10} and C_{11} are comparable in magnitude. The divergences of C_0 and C_{11} as $h_x/J_z \to 2$ arise because $|\bar{\chi}_2|$ approaches zero.

IV. DISCUSSION

The most significant assumption in our theory is the linear approximation of the third-order susceptibility, as given in Eqs. (29) and (30). Provided this approximation holds, Eq. (35) offers a quantitative estimate of the SH intensity change and should be valid even in more complex systems, including real materials. In the MF transverse-field Ising model discussed in Sec. III, by considering the h_x dependence of Eqs. (46) and (47), we suppose that C_0 vanishes when the magnitude of the polarization expectation value $\langle 0|P|0\rangle$ becomes comparable to that of the transition dipole moment $\langle 0|P|1\rangle$. However, the universality of this behavior is still an open question. It is therefore important to apply our formulas to other systems to determine whether the time-derivative component can dominate and whether $\Delta I_{\mathrm{SH}}(t)$ remains in phase with $E_{\mathrm{THz}}(t)$.

If one extends beyond the linear approximation to include second-order terms, Eq. (25) yields contributions of the form $\omega^2(\omega \mp 2\omega_{\mathrm{IR}})^2 E_{\mathrm{THz}}(\omega \mp 2\omega_{\mathrm{IR}})$, which in the time domain correspond to second- and higher-order time derivatives of $E_{\mathrm{THz}}(t)$. Experimental detection of these contributions would be highly challenging with current experimental capabilities. Additionally, if ΔI_{SH} depends nonlinearly on E_{THz}, the present formulation breaks down, and a higher-order perturbative expansion becomes necessary. However, there is no reason to expect that the simple relation $\Delta P \propto \Delta I_{\mathrm{SH}}$ holds in such strongly nonlinear regimes.

In this work, we have discussed the modulation of the polarization and the SH intensity by an external electric field pulse. Other intriguing second-order phenomena, such as optical rectification and the bulk photovoltaic effect, are also

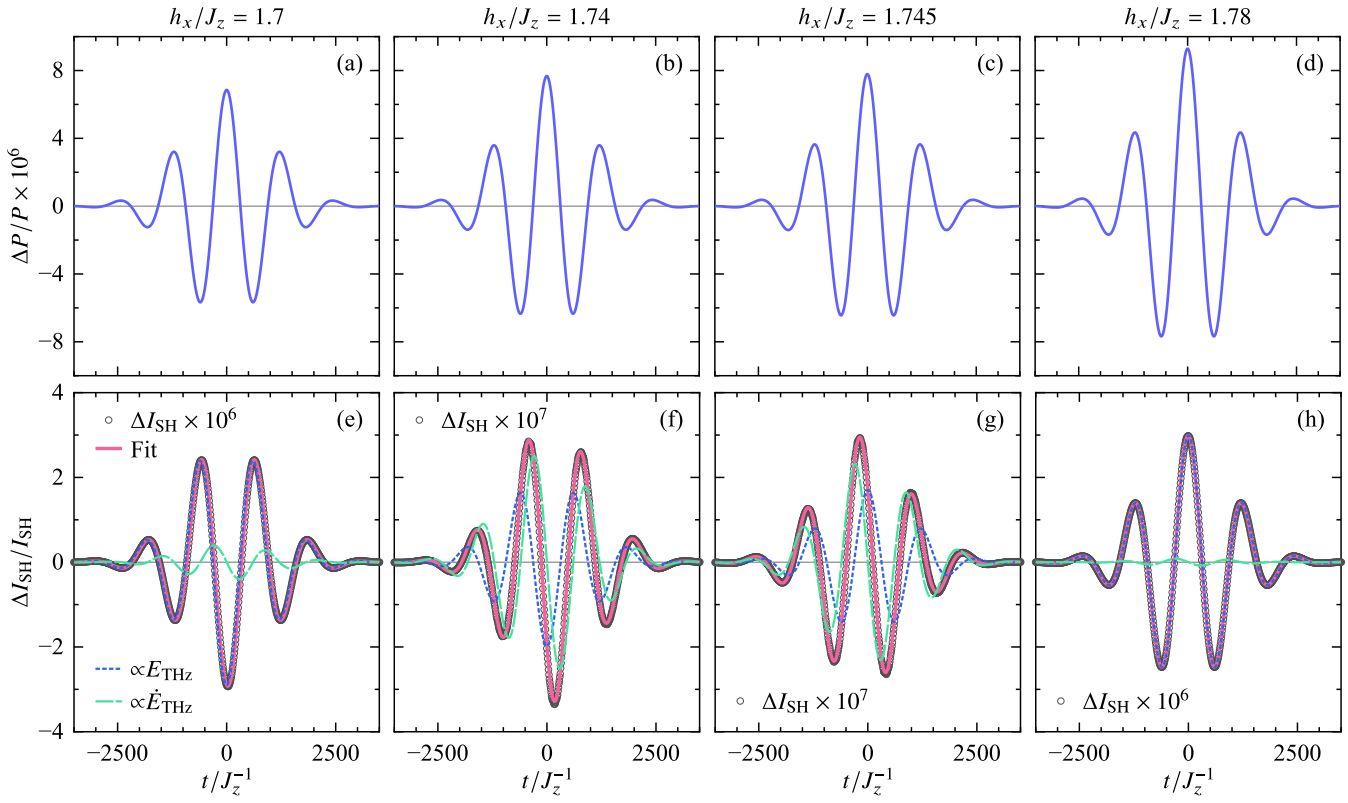


FIG. 4. Relative changes in (a)–(d) the electric polarization $\Delta P/P$ and (e)–(h) the SH intensity $\Delta I_{\rm SH}/I_{\rm SH}$, for $h_x/J_z = 1.7$, 1.74, 1.745, and 1.78 (left to right). The solid red curves represent fitted results, along with their $E_{\rm THz}(t)$ component (dotted blue) and $\dot{E}_{\rm THz}(t)$ component (dashed green).

described by the second-order response function. Similarly, the linear modulation of these effects can be described by the third-order susceptibility. Although in Eqs. (21) and (22) we focused on contributions around $\omega \approx \pm 2\omega_{\rm IR}$, an analogous discussion could address the response near $\omega \approx 0$. However, when considering a monochromatic probe as in Eq. (17), the far field E_∞ in Eq. (24) vanishes at $\omega = 0$, and thus the theory would require some modifications. A detailed investigation of this aspect is left for future work.

V. SUMMARY

We investigated the temporal modulation of the electric polarization $\Delta P(t)$ and second harmonic intensity $\Delta I_{\rm SH}(t)$, both of which are linearly induced by a low-frequency electric field pulse $E_{\rm THz}(t)$. Using nonlinear response theory, we derived general expressions for ΔP and $\Delta I_{\rm SH}$, demonstrating that $\Delta I_{\rm SH}$ can contain terms proportional not only to $E_{\rm THz}(t)$ but also to its time derivative $\dot{E}_{\rm THz}(t)$. Through an analysis of

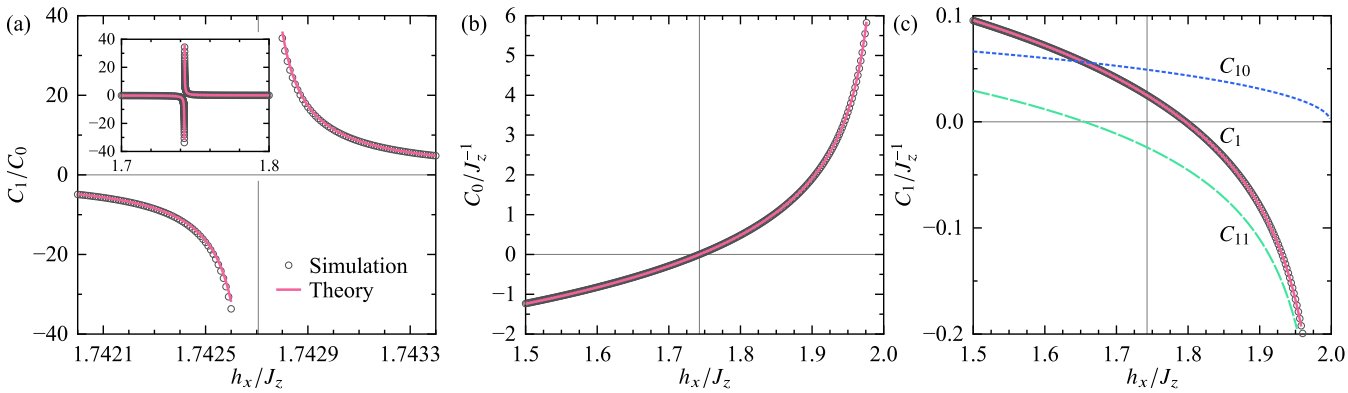


FIG. 5. (a) Ratio C_1/C_0 representing the relative contribution of the time-derivative component. The inset shows a broader view for $h_x/J_z \in [1.7, 1.8]$. The circular markers show the results of the real-time simulations, and the solid red curve indicates the theoretical values calculated from Eqs. (37)–(39). [(b) and (c)] Weight of the component proportional to (b) $E_{\rm THz}$ and (c) $\dot{E}_{\rm THz}/\omega_{\rm THz}$. The gray vertical lines in (a)–(c) indicate $h_x/J_z = 1.742\,706\,2$, at which C_0 vanishes.

the transverse-field Ising model within the mean-field approximation, we showed that for most parameter regimes, $\Delta I_{\rm SH}$ is predominantly proportional to $E_{\rm THz}(t)$, in agreement with common assumptions. We also found that the time-derivative component can become significant under certain conditions, and our simulations quantitatively agree with the theoretical predictions. Furthermore, we showed that when the time-derivative component is negligible, $\Delta I_{\rm SH}$ can nonetheless be in antiphase with $E_{\rm THz}(t)$; that is, $\Delta I_{\rm SH}$ can decrease while ΔP increases, and vice versa. These findings reveal that the commonly assumed relation $\Delta P(t) \propto \Delta I_{\rm SH}(t)$ does not always hold, thereby enabling a more accurate analysis of the ultrafast dynamics in ferroelectrics driven by electric field pulses.

ACKNOWLEDGMENTS

The author is grateful to Shinichiro Iwai, Hirotake Itoh, Yoichi Okimoto, and Shin-ya Koshihara for their insightful comments in the early stages of this work. This work was supported by JSPS KAKENHI Grants No. JP23K13052, No. JP23K25805, and No. JP24K00563. The numerical calculations were performed using the facilities of the Supercomputer Center, the Institute for Solid State Physics, the University of Tokyo.

DATA AVAILABILITY

The data that support the findings of this article are not publicly available upon publication because it is not technically feasible and/or the cost of preparing, depositing, and hosting the data would be prohibitive within the terms of this research project. The data are available from the authors upon reasonable request.

APPENDIX: SPECTRAL REPRESENTATION OF NONLINEAR SUSCEPTIBILITY

We present the spectral representation of the second- and third-order susceptibilities [96]. Let $\mathcal{H}_0$ be the unperturbed Hamiltonian, with its many-body eigenstates $\{|n\rangle\}$ and eigenenergies $\{\varepsilon_n\}$. The ground state of $\mathcal{H}_0$ is denoted by $|0\rangle$. For generality, we consider a set of physical quantities $\{Q^\alpha\}$ that are linearly coupled to external fields $\{f_\beta(t)\}$ as

$$\mathcal{V}(t) = -\sum_\beta Q^\beta f_\beta(t). \tag{A1}$$

The nonlinear response function is generally expressed as

$$\begin{aligned}&\chi^{(n)}_{\alpha\beta_1\cdots\beta_n}(t;t_1,t_2,\ldots,t_n)\\&\quad= \mathrm{i}^n\Theta(t-t_1)\Theta(t_1-t_2)\cdots\Theta(t_{n-1}-t_n)\\&\qquad\times\left\langle[[\cdots[[\hat{Q}^\alpha(t),\hat{Q}^{\beta_1}(t_1)],\hat{Q}^{\beta_2}(t_2)],\cdots],\hat{Q}^{\beta_n}(t_n)]\right\rangle_0.\end{aligned} \tag{A2}$$

By inserting the resolution of the identity, $1=\sum_n |n\rangle\langle n|$, into Eq. (A2) and performing the Fourier transformation, we obtain the expression for the second-order response function in the ground state as

$$\begin{aligned}\chi^{(2)}_{\alpha\beta_1\beta_2}(\omega_1,\omega_2) = \sum_{mn}\Bigg[&\frac{Q^\alpha_{0m}Q^{\beta_1}_{mn}Q^{\beta_2}_{n0}}{(\omega_1^+ + \omega_2^+ - \varepsilon_m + \varepsilon_0)(\omega_2^+ - \varepsilon_n + \varepsilon_0)}\\&+\frac{Q^{\beta_2}_{0m}Q^{\beta_1}_{mn}Q^{\alpha}_{n0}}{(\omega_1^+ + \omega_2^+ - \varepsilon_0 + \varepsilon_n)(\omega_2^+ - \varepsilon_0 + \varepsilon_m)}\\&-\frac{Q^{\beta_2}_{0m}Q^{\alpha}_{mn}Q^{\beta_1}_{n0}}{(\omega_1^+ + \omega_2^+ - \varepsilon_n + \varepsilon_m)(\omega_2^+ - \varepsilon_0 + \varepsilon_m)}\\&-\frac{Q^{\beta_1}_{0m}Q^{\alpha}_{mn}Q^{\beta_2}_{n0}}{(\omega_1^+ + \omega_2^+ - \varepsilon_n + \varepsilon_m)(\omega_2^+ - \varepsilon_n + \varepsilon_0)}\Bigg],\end{aligned} \tag{A3}$$

with $Q^\alpha_{mn} = \langle m|Q^\alpha|n\rangle$. Similarly, the spectral representation of the third-order response function is given by

$$\begin{aligned}&\chi^{(3)}_{\alpha\beta_1\beta_2\beta_3}(\omega_1,\omega_2,\omega_3)\\&=\sum_{lmn}\Bigg[-\frac{Q^\alpha_{0l}Q^{\beta_1}_{lm}Q^{\beta_2}_{mn}Q^{\beta_3}_{n0}}{(\omega_1^+ + \omega_2^+ + \omega_3^+ - \varepsilon_{l0})(\omega_2^+ + \omega_3^+ - \varepsilon_{m0})(\omega_3^+ - \varepsilon_{n0})}\\&+\frac{Q^{\beta_3}_{0l}Q^{\beta_2}_{lm}Q^{\beta_1}_{mn}Q^{\alpha}_{n0}}{(\omega_1^+ + \omega_2^+ + \omega_3^+ - \varepsilon_{0n})(\omega_2^+ + \omega_3^+ - \varepsilon_{0m})(\omega_3^+ - \varepsilon_{0l})}\\&+\frac{Q^{\beta_1}_{0l}Q^{\alpha}_{lm}Q^{\beta_2}_{mn}Q^{\beta_3}_{n0}}{(\omega_1^+ + \omega_2^+ + \omega_3^+ - \varepsilon_{ml})(\omega_2^+ + \omega_3^+ - \varepsilon_{m0})(\omega_3^+ - \varepsilon_{n0})}\\&+\frac{Q^{\beta_2}_{0l}Q^{\alpha}_{lm}Q^{\beta_1}_{mn}Q^{\beta_3}_{n0}}{(\omega_1^+ + \omega_2^+ + \omega_3^+ - \varepsilon_{ml})(\omega_2^+ + \omega_3^+ - \varepsilon_{nl})(\omega_3^+ - \varepsilon_{n0})}\\&+\frac{Q^{\beta_3}_{0l}Q^{\alpha}_{lm}Q^{\beta_1}_{mn}Q^{\beta_2}_{n0}}{(\omega_1^+ + \omega_2^+ + \omega_3^+ - \varepsilon_{ml})(\omega_2^+ + \omega_3^+ - \varepsilon_{nl})(\omega_3^+ - \varepsilon_{0l})}\\&-\frac{Q^{\beta_3}_{0l}Q^{\beta_2}_{lm}Q^{\alpha}_{mn}Q^{\beta_1}_{n0}}{(\omega_1^+ + \omega_2^+ + \omega_3^+ - \varepsilon_{nm})(\omega_2^+ + \omega_3^+ - \varepsilon_{0m})(\omega_3^+ - \varepsilon_{0l})}\\&-\frac{Q^{\beta_3}_{0l}Q^{\beta_1}_{lm}Q^{\alpha}_{mn}Q^{\beta_2}_{n0}}{(\omega_1^+ + \omega_2^+ + \omega_3^+ - \varepsilon_{nm})(\omega_2^+ + \omega_3^+ - \varepsilon_{nl})(\omega_3^+ - \varepsilon_{0l})}\\&-\frac{Q^{\beta_2}_{0l}Q^{\beta_1}_{lm}Q^{\alpha}_{mn}Q^{\beta_3}_{n0}}{(\omega_1^+ + \omega_2^+ + \omega_3^+ - \varepsilon_{nm})(\omega_2^+ + \omega_3^+ - \varepsilon_{nl})(\omega_3^+ - \varepsilon_{n0})}\Bigg],\end{aligned} \tag{A4}$$

where $\varepsilon_{mn} = \varepsilon_m - \varepsilon_n$. In Eqs. (A3) and (A4), ω_i^+ denotes a complex frequency with a positive imaginary part. It was shown in Ref. [97] that applying the following substitution yields good agreement between the nonlinear responses obtained from real-time simulations and those derived from the spectral representation:

$$\omega_3^+ \to \omega_3 + \mathrm{i}\eta, \tag{A5}$$

$$\omega_2^+ + \omega_3^+ \to \omega_2 + \omega_3 + \mathrm{i}\eta, \tag{A6}$$

$$\omega_1^+ + \omega_2^+ + \omega_3^+ \to \omega_1 + \omega_2 + \omega_3 + \mathrm{i}\eta, \tag{A7}$$

where η is set to the relaxation rate in Eq. (55), i.e., $\eta = \Gamma$. Additionally, the nonlinear susceptibilities in Eqs. (A3) and (A4) need to be symmetrized in accordance with Eq. (23).

[1] P. A. Franken, A. E. Hill, C. W. Peters, and G. Weinreich, Generation of optical harmonics, Phys. Rev. Lett. **7**, 118 (1961).

[2] J. A. Armstrong, N. Bloembergen, J. Ducuing, and P. S. Pershan, Interactions between light waves in a nonlinear dielectric, Phys. Rev. **127**, 1918 (1962).

[3] P. A. Franken and J. F. Ward, Optical harmonics and nonlinear phenomena, Rev. Mod. Phys. **35**, 23 (1963).

[4] Y. R. Shen, Surface properties probed by second-harmonic and sum-frequency generation, Nature (London) **337**, 519 (1989).

[5] M. Fiebig, V. V. Pavlov, and R. V. Pisarev, Second-harmonic generation as a tool for studying electronic and magnetic structures of crystals: review, J. Opt. Soc. Am. B **22**, 96 (2005).

[6] H. Ma, J. Liang, H. Hong, K. Liu, D. Zou, M. Wu, and K. Liu, Rich information on 2D materials revealed by optical second harmonic generation, Nanoscale **12**, 22891 (2020).

[7] A. Kirilyuk, A. V. Kimel, and T. Rasing, Ultrafast optical manipulation of magnetic order, Rev. Mod. Phys. **82**, 2731 (2010).

[8] S. K. Kurtz and T. T. Perry, A powder technique for the evaluation of nonlinear optical materials, J. Appl. Phys. **39**, 3798 (1968).

[9] Y. Uesu, S. Kurimura, and Y. Yamamoto, Optical second harmonic images of 90° domain structure in $BaTiO_3$ and periodically inverted antiparallel domains in $LiTaO_3$, Appl. Phys. Lett. **66**, 2165 (1995).

[10] M. Trassin, G. D. Luca, S. Manz, and M. Fiebig, Probing ferroelectric domain engineering in $BiFeO_3$ thin films by second harmonic generation, Adv. Mater. **27**, 4871 (2015).

[11] Y. Zhang, Y. Zhang, Q. Guo, X. Zhong, Y. Chu, H. Lu, G. Zhong, J. Jiang, C. Tan, M. Liao, Z. Lu, D. Zhang, J. Wang, J. Yuan, and Y. Zhou, Characterization of domain distributions by second harmonic generation in ferroelectrics, npj Comput. Mater. **4**, 39 (2018).

[12] K. J. Spychala, P. Mackwitz, M. Rüsing, A. Widhalm, G. Berth, C. Silberhorn, and A. Zrenner, Nonlinear focal mapping of ferroelectric domain walls in $LiNbO_3$: Analysis of the SHG microscopy contrast mechanism, J. Appl. Phys. **128**, 234102 (2020).

[13] K. Fujiwara, Y. Fukada, Y. Okuda, R. Seimiya, N. Ikeda, K. Yokoyama, H. Yu, S. Koshihara, and Y. Okimoto, Direct evidence of electronic ferroelectricity in $YbFe_2O_4$ using neutron diffraction and nonlinear spectroscopy, Sci. Rep. **11**, 4277 (2021).

[14] I. Abdelwahab, B. Tilmann, Y. Wu, D. Giovanni, I. Verzhbitskiy, M. Zhu, R. Berté, F. Xuan, L. de S. Menezes, G. Eda, T. C. Sum, S. Y. Quek, S. A. Maier, and K. P. Loh, Giant second-harmonic generation in ferroelectric $NbOI_2$, Nat. Photon. **16**, 644 (2022).

[15] P. A. Hegarty, H. Beccard, L. M. Eng, and M. Rüsing, Turn all the lights off: Bright- and dark-field second-harmonic microscopy to select contrast mechanisms for ferroelectric domain walls, J. Appl. Phys. **131**, 244102 (2022).

[16] M. Fiebig, T. Lottermoser, D. Meier, and M. Trassin, The evolution of multiferroics, Nat. Rev. Mater. **1**, 16046 (2016).

[17] T. Lottermoser, T. Lonkai, U. Amann, D. Hohlwein, J. Ihringer, and M. Fiebig, Magnetic phase control by an electric field, Nature (London) **430**, 541 (2004).

[18] A. Sharan, J. Lettieri, Y. Jia, W. Tian, X. Pan, D. G. Schlom, and V. Gopalan, Bismuth manganite: A multiferroic with a large nonlinear optical response, Phys. Rev. B **69**, 214109 (2004).

[19] W. Jin, E. Drueke, S. Li, A. Admasu, R. Owen, M. Day, K. Sun, S.-W. Cheong, and L. Zhao, Observation of a ferro-rotational order coupled with second-order nonlinear optical fields, Nat. Phys. **16**, 42 (2020).

[20] S. Toyoda, M. Fiebig, T.-H. Arima, Y. Tokura, and N. Ogawa, Nonreciprocal second harmonic generation in a magnetoelectric material, Sci. Adv. **7**, eabe2793 (2021).

[21] S. Xu, J. Wang, P. Chen, K. Jin, C. Ma, S. Wu, E.-J. Guo, C. Ge, C. Wang, X. Xu, H. Yao, J. Wang, D. Xie, X. Wang, K. Chang, X. Bai, and G. Yang, Magnetoelectric coupling in multiferroics probed by optical second harmonic generation, Nat. Commun. **14**, 2274 (2023).

[22] B. B. Prasad, G.-f. Liu, and G.-y. Guo, Magnetism-induced second-order nonlinear optical responses in multiferroic $BiFeO_3$, Phys. Rev. B **110**, 014422 (2024).

[23] P. Němec, M. Fiebig, T. Kampfrath, and A. V. Kimel, Antiferromagnetic opto-spintronics, Nat. Phys. **14**, 229 (2018).

[24] J. Hohlfeld, E. Matthias, R. Knorren, and K. H. Bennemann, Nonequilibrium magnetization dynamics of nickel, Phys. Rev. Lett. **78**, 4861 (1997).

[25] M. Fiebig, D. Fröhlich, T. Lottermoser, V. V. Pavlov, R. V. Pisarev, and H.-J. Weber, Second harmonic generation in the centrosymmetric antiferromagnet NiO, Phys. Rev. Lett. **87**, 137202 (2001).

[26] V. V. Pavlov, A. M. Kalashnikova, R. V. Pisarev, I. Sänger, D. R. Yakovlev, and M. Bayer, Magnetic-field-induced second-harmonic generation in semiconductor GaAs, Phys. Rev. Lett. **94**, 157404 (2005).

[27] C. Tzschaschel, T. Satoh, and M. Fiebig, Tracking the ultrafast motion of an antiferromagnetic order parameter, Nat. Commun. **10**, 3995 (2019).

[28] S. Okumura, T. Morimoto, Y. Kato, and Y. Motome, Quadratic optical responses in a chiral magnet, Phys. Rev. B **104**, L180407 (2021).

[29] R.-C. Xiao, D.-F. Shao, W. Gan, H.-W. Wang, H. Han, Z. G. Sheng, C. Zhang, H. Jiang, and H. Li, Classification of second harmonic generation effect in magnetically ordered materials, npj Quantum Mater. **8**, 62 (2023).

[30] S. Toyoda, J.-C. Liao, G.-Y. Guo, Y. Tokunaga, T.-h. Arima, Y. Tokura, and N. Ogawa, Magnetic-field switching of second-harmonic generation in noncentrosymmetric magnet $Eu_2MnSi_2O_7$, Phys. Rev. Mater. **7**, 024403 (2023).

[31] K. Shoriki, K. Moriishi, Y. Okamura, K. Yokoi, H. Usui, H. Murakawa, H. Sakai, N. Hanasaki, Y. Tokura, and Y. Takahashi, Large nonlinear optical magnetoelectric response in a noncentrosymmetric magnetic Weyl semimetal, Proc. Natl. Acad. Sci. USA **121**, e2316910121 (2024).

[32] D. Wu, M. Ye, H. Chen, Y. Xu, and W. Duan, Giant and controllable nonlinear magneto-optical effects in two-dimensional magnets, npj Comput. Mater. **10**, 79 (2024).

[33] D. Wu, Y. Xu, M. Ye, and W. Duan, Spin-chirality-driven second-harmonic generation in two-dimensional magnet CrSBr, Sci. Adv. **11**, eadu6562 (2025).

[34] N. Kumar, S. Najmaei, Q. Cui, F. Ceballos, P. M. Ajayan, J. Lou, and H. Zhao, Second harmonic microscopy of monolayer MoS_2, Phys. Rev. B **87**, 161403(R) (2013).

[35] Y. Li, Y. Rao, K. F. Mak, Y. You, S. Wang, C. R. Dean, and T. F. Heinz, Probing symmetry properties of few-layer MoS_2 and h-BN by optical second-harmonic generation, Nano Lett. **13**, 3329 (2013).

[36] K. L. Seyler, J. R. Schaibley, P. Gong, P. Rivera, A. M. Jones, S. Wu, J. Yan, D. G. Mandrus, W. Yao, and X. Xu, Electrical control of second-harmonic generation in a WSe_2 monolayer transistor, Nat. Nanotechnol. **10**, 407 (2015).

[37] P. Herrmann, S. Klimmer, T. Lettau, T. Weickhardt, A. Papavasileiou, K. Mosina, Z. Sofer, I. Paradisanos, D. Kartashov, J. Wilhelm, and G. Soavi, Nonlinear valley selection rules and all-optical probe of broken time-reversal symmetry in monolayer WSe_2, Nat. Photon. **19**, 300 (2025).

[38] J. Orenstein, J. E. Moore, T. Morimoto, D. H. Torchinsky, J. W. Harter, and D. Hsieh, Topology and symmetry of quantum materials via nonlinear optical responses, Annu. Rev. Condens. Matter Phys. **12**, 247 (2021).

[39] Z. Hu and G. Li, Nonlinear geometric phase in optics: Fundamentals and applications, Appl. Phys. Lett. **126**, 100502 (2025).

[40] T. Morimoto and N. Nagaosa, Topological nature of nonlinear optical effects in solids, Sci. Adv. **2**, e1501524 (2016).

[41] L. Wu, S. Patankar, T. Morimoto, N. L. Nair, E. Thewalt, A. Little, J. G. Analytis, J. E. Moore, and J. Orenstein, Giant anisotropic nonlinear optical response in transition metal monopnictide Weyl semimetals, Nat. Phys. **13**, 350 (2017).

[42] Z. Li, Y.-Q. Jin, T. Tohyama, T. Iitaka, J.-X. Zhang, and H. Su, Second harmonic generation in the Weyl semimetal TaAs from a quantum kinetic equation, Phys. Rev. B **97**, 085201 (2018).

[43] S. Patankar, L. Wu, B. Lu, M. Rai, J. D. Tran, T. Morimoto, D. E. Parker, A. G. Grushin, N. L. Nair, J. G. Analytis, J. E. Moore, J. Orenstein, and D. H. Torchinsky, Resonance-enhanced optical nonlinearity in the Weyl semimetal TaAs, Phys. Rev. B **98**, 165113 (2018).

[44] P. Bhalla, K. Das, D. Culcer, and A. Agarwal, Resonant second-harmonic generation as a probe of quantum geometry, Phys. Rev. Lett. **129**, 227401 (2022).

[45] H. Watanabe, A. Daido, and Y. Yanase, Nonreciprocal optical response in parity-breaking superconductors, Phys. Rev. B **105**, 024308 (2022).

[46] H. Tanaka, H. Watanabe, and Y. Yanase, Nonlinear optical response in superconductors in magnetic field: Quantum geometry and topological superconductivity, Phys. Rev. B **110**, 014520 (2024).

[47] C. Tzschaschel, J.-X. Qiu, X.-J. Gao, H.-C. Li, C. Guo, H.-Y. Yang, C.-P. Zhang, Y.-M. Xie, Y.-F. Liu, A. Gao, D. Bérubé, T. Dinh, S.-C. Ho, Y. Fang, F. Huang, J. Nordlander, Q. Ma, F. Tafti, P. J. W. Moll, K. T. Law, and S.-Y. Xu, Nonlinear optical diode effect in a magnetic Weyl semimetal, Nat. Commun. **15**, 3017 (2024).

[48] P. He, H. Isobe, D. Zhu, C.-H. Hsu, L. Fu, and H. Yang, Quantum frequency doubling in the topological insulator Bi_2Se_3, Nat. Commun. **12**, 698 (2021).

[49] I. Sodemann and L. Fu, Quantum nonlinear Hall effect induced by Berry curvature dipole in time-reversal invariant materials, Phys. Rev. Lett. **115**, 216806 (2015).

[50] M. S. Okyay, S. A. Sato, K. W. Kim, B. Yan, H. Jin, and N. Park, Second harmonic Hall responses of insulators as a probe of Berry curvature dipole, Commun. Phys. **5**, 303 (2022).

[51] K. S. Denisov, Y. Liu, and I. Žutić, Movable Dirac points with ferroelectrics: Kink states and Berry curvature dipoles, Phys. Rev. Lett. **134**, 246602 (2025).

[52] X. Li, T. Qiu, J. Zhang, E. Baldini, J. Lu, A. M. Rappe, and K. A. Nelson, Terahertz field–induced ferroelectricity in quantum paraelectric $SrTiO_3$, Science **364**, 1079 (2019).

[53] T. F. Nova, A. S. Disa, M. Fechner, and A. Cavalleri, Metastable ferroelectricity in optically strained $SrTiO_3$, Science **364**, 1075 (2019).

[54] D. Shin, S. Latini, C. Schäfer, S. A. Sato, E. Baldini, U. De Giovannini, H. Hübener, and A. Rubio, Simulating terahertz field-induced ferroelectricity in quantum paraelectric $SrTiO_3$, Phys. Rev. Lett. **129**, 167401 (2022).

[55] X. Li, P. Peng, H. Dammak, G. Geneste, A. Akbarzadeh, S. Prosandeev, L. Bellaiche, and D. Talbayev, Terahertz pulse induced second harmonic generation and Kerr effect in the quantum paraelectric $KTaO_3$, Phys. Rev. B **107**, 064306 (2023).

[56] V. Bilyk, K. Brekhov, A. Ovchinnikov, O. Chefonov, and E. Mishina, Terahertz-induced polar state in quantum paraelectric $SrTiO_3$, MRS Adv. **8**, 943 (2023).

[57] F. Yang, X. J. Li, D. Talbayev, and L. Q. Chen, Terahertz-induced second-harmonic generation in quantum paraelectrics: Hot-phonon effect, Phys. Rev. Lett. **135**, 056901 (2025).

[58] T. Miyamoto, H. Yada, H. Yamakawa, and H. Okamoto, Ultrafast modulation of polarization amplitude by terahertz fields in electronic-type organic ferroelectrics, Nat. Commun. **4**, 2586 (2013).

[59] H. Yamakawa, T. Miyamoto, T. Morimoto, H. Yada, Y. Kinoshita, M. Sotome, N. Kida, K. Yamamoto, K. Iwano, Y. Matsumoto, S. Watanabe, Y. Shimoi, M. Suda, H. M. Yamamoto, H. Mori, and H. Okamoto, Novel electronic ferroelectricity in an organic charge-order insulator investigated with terahertz-pump optical-probe spectroscopy, Sci. Rep. **6**, 20571 (2016).

[60] K. Iwano, Y. Shimoi, T. Miyamoto, D. Hata, M. Sotome, N. Kida, S. Horiuchi, and H. Okamoto, Ultrafast photoinduced electric-polarization switching in a hydrogen-bonded ferroelectric crystal, Phys. Rev. Lett. **118**, 107404 (2017).

[61] T. Morimoto, T. Miyamoto, H. Yamakawa, T. Terashige, T. Ono, N. Kida, and H. Okamoto, Terahertz-field-induced large macroscopic polarization and domain-wall dynamics in an organic molecular dielectric, Phys. Rev. Lett. **118**, 107602 (2017).

[62] T. Miyamoto, D. Hata, T. Morimoto, H. Yamakawa, N. Kida, T. Terashige, K. Iwano, H. Kishida, S. Horiuchi, and H. Okamoto, Ultrafast polarization control by terahertz fields via π-electron wavefunction changes in hydrogen-bonded molecular ferroelectrics, Sci. Rep. **8**, 15014 (2018).

[63] H. Yamakawa, T. Miyamoto, T. Morimoto, N. Takamura, S. Liang, H. Yoshimochi, T. Terashige, N. Kida, M. Suda, H. M. Yamamoto, H. Mori, K. Miyagawa, K. Kanoda, and H. Okamoto, Terahertz-field-induced polar charge order in electronic-type dielectrics, Nat. Commun. **12**, 953 (2021).

[64] N. Kida, T. Miyamoto, and H. Okamoto, Emission of terahertz electromagnetic waves: A new spectroscopic method to investigate physical properties of solids, J. Phys. Soc. Jpn. **91**, 112001 (2022).

[65] T. Umanodan, K. Kaneshima, K. Takeuchi, N. Ishii, J. Itatani, H. Hirori, Y. Sanari, K. Tanaka, Y. Kanemitsu, T. Ishikawa, S.-y. Koshihara, S. Horiuchi, and Y. Okimoto, Ultrafast control of ferroelectricity with dynamical repositioning of protons in a supramolecular cocrystal studied by femtosecond nonlinear spectroscopy, J. Phys. Soc. Jpn. **88**, 013705 (2019).

[66] A. Sugisawa, T. Umanodan, H. Yu, T. Ishikawa, S.-y. Koshihara, S. Horiuchi, and Y. Okimoto, Ultrafast variation of the polarized state in proton-π electron coupled ferroelectric cocrystal Phz-H_2ca, Mater. Adv. **4**, 5126 (2023).

[67] R. Mankowsky, A. von Hoegen, M. Först, and A. Cavalleri, Ultrafast reversal of the ferroelectric polarization, Phys. Rev. Lett. **118**, 197601 (2017).

[68] K. A. Grishunin, N. A. Ilyin, N. E. Sherstyuk, E. D. Mishina, A. Kimel, V. M. Mukhortov, A. V. Ovchinnikov, O. V. Chefonov, and M. B. Agranat, THz electric field-induced second harmonic generation in inorganic ferroelectric, Sci. Rep. **7**, 687 (2017).

[69] K. Grishunin, V. Bilyk, N. Sherstyuk, V. Mukhortov, A. Ovchinnikov, O. Chefonov, M. Agranat, E. Mishina, and A. V. Kimel, Transient second harmonic generation induced by single cycle THz pulses in $Ba_{0.8}Sr_{0.2}TiO_3$/MgO, Sci. Rep. **9**, 697 (2019).

[70] F. Chen, J. Goodfellow, S. Liu, I. Grinberg, M. C. Hoffmann, A. R. Damodaran, Y. Zhu, P. Zalden, X. Zhang, I. Takeuchi, A. M. Rappe, L. W. Martin, H. Wen, and A. M. Lindenberg, Ultrafast terahertz gating of the polarization and giant nonlinear optical response in $BiFeO_3$ thin films, Adv. Mater. **27**, 6371 (2015).

[71] H. Yu, K. Takubo, T. Ishikawa, S.-y. Koshihara, M. Hada, T. Asaka, K. Ozawa, K. Shigematsu, M. Azuma, and Y. Okimoto, Ultrafast nonlinear spectroscopy in (111) oriented bismuth ferrite oxide, J. Phys. Soc. Jpn. **89**, 063401 (2020).

[72] H. Yu, Y. Fukada, G. Nishida, K. Takubo, T. Ishikawa, S. Koshihara, N. Ikeda, and Y. Okimoto, Ultrafast anisotropic polarization dynamics of electronic ferroelectric $LuFe_2O_4$, Phys. Rev. Mater. **8**, 064402 (2024).

[73] K. Takubo, A. Ono, S. Ueno, S. Banu, H. Yu, K. En-ya, R. Nishimori, M. Kuwahara, T. Asaka, K. Maeda, D. Ono, K. Ozawa, T. Itoh, K. Shigematsu, M. Azuma, T. Ishikawa, Y. Okimoto, M. Hada, and S.-y. Koshihara, Photocontrol of ferroelectricity in multiferroic $BiFeO_3$ via structural modification coupled with photocarrier, Commun. Mater. **5**, 261 (2024).

[74] H. Itoh, R. Minakami, H. Yu, R. Tsuruoka, T. Amano, Y. Kawakami, S.-y. Koshihara, K. Fujiwara, N. Ikeda, Y. Okimoto, and S. Iwai, Terahertz field control of electronic-ferroelectric anisotropy at room temperature in $LuFe_2O_4$, Phys. Rev. Lett. **135**, 106504 (2025).

[75] Y. M. Sheu, N. Ogawa, Y. Kaneko, and Y. Tokura, Photocreating supercooled spiral-spin states in a multiferroic manganite, Phys. Rev. B **94**, 081107(R) (2016).

[76] M. Matsubara, Ultrafast optical control of magnetic interactions in carrier-density-controlled ferromagnetic semiconductors, Appl. Sci. **9**, 948 (2019).

[77] D. A. Bustamante Lopez, D. M. Juraschek, M. Fechner, X. Xu, S.-W. Cheong, and W. Hu, Ultrafast simultaneous manipulation of multiple ferroic orders through nonlinear phonon excitation, npj Quantum Mater. **10**, 24 (2025).

[78] R. W. Terhune, P. D. Maker, and C. M. Savage, Optical harmonic generation in calcite, Phys. Rev. Lett. **8**, 404 (1962).

[79] E. J. Sie, C. M. Nyby, C. D. Pemmaraju, S. J. Park, X. Shen, J. Yang, M. C. Hoffmann, B. K. Ofori-Okai, R. Li, A. H. Reid, S. Weathersby, E. Mannebach, N. Finney, D. Rhodes, D. Chenet, A. Antony, L. Balicas, J. Hone, T. P. Devereaux, T. F. Heinz, X. Wang, and A. M. Lindenberg, An ultrafast symmetry switch in a Weyl semimetal, Nature (London) **565**, 61 (2019).

[80] C. Vaswani, M. Mootz, C. Sundahl, D. H. Mudiyanselage, J. H. Kang, X. Yang, D. Cheng, C. Huang, R. H. J. Kim, Z. Liu, L. Luo, I. E. Perakis, C. B. Eom, and J. Wang, Terahertz second-harmonic generation from lightwave acceleration of symmetry-breaking nonlinear supercurrents, Phys. Rev. Lett. **124**, 207003 (2020).

[81] A. V. Ovchinnikov, O. V. Chefonov, E. D. Mishina, and M. B. Agranat, Second harmonic generation in the bulk of silicon induced by an electric field of a high power terahertz pulse, Sci. Rep. **9**, 9753 (2019).

[82] M. Tokman, S. B. Bodrov, Y. A. Sergeev, A. I. Korytin, I. Oladyshkin, Y. Wang, A. Belyanin, and A. N. Stepanov, Second harmonic generation in graphene dressed by a strong terahertz field, Phys. Rev. B **99**, 155411 (2019).

[83] Y. Kawakami, T. Amano, H. Ohashi, H. Itoh, Y. Nakamura, H. Kishida, T. Sasaki, G. Kawaguchi, H. M. Yamamoto, K. Yamamoto, S. Ishihara, K. Yonemitsu, and S. Iwai, Petahertz non-linear current in a centrosymmetric organic superconductor, Nat. Commun. **11**, 4138 (2020).

[84] K. Takasan, T. Morimoto, J. Orenstein, and J. E. Moore, Current-induced second harmonic generation in inversion-symmetric Dirac and Weyl semimetals, Phys. Rev. B **104**, L161202 (2021).

[85] Y. Gao and F. Zhang, Current-induced second harmonic generation of Dirac or Weyl semimetals in a strong magnetic field, Phys. Rev. B **103**, L041301 (2021).

[86] S. Nakamura, K. Katsumi, H. Terai, and R. Shimano, Nonreciprocal terahertz second-harmonic generation in superconducting NbN under supercurrent injection, Phys. Rev. Lett. **125**, 097004 (2020).

[87] S. Nakamura, H. Matsumoto, H. Ogawa, T. Kobayashi, F. Nabeshima, A. Maeda, and R. Shimano, Picosecond trajectory of two-dimensional vortex motion in $FeSe_{0.5}Te_{0.5}$ visualized by terahertz second harmonic generation, Phys. Rev. Lett. **133**, 036004 (2024).

[88] S. Wang, W. Li, C. Deng, Z. Hong, H.-b. Gao, X. Li, Y. Gu, Q. Zheng, Y. Wu, P. G. Evans, J.-F. Li, C.-w. Nan, and Q. Li, Giant electric field-induced second harmonic generation in polar skyrmions, Nat. Commun. **15**, 1374 (2024).

[89] C. Timm and K. H. Bennemann, Response theory for time-resolved second-harmonic generation and two-photon photoemission, J. Phys.: Condens. Matter **16**, 661 (2004).

[90] S. Ishihara, Electronic ferroelectricity and frustration, J. Phys. Soc. Jpn. **79**, 011010 (2010).

[91] N. Ikeda, H. Ohsumi, K. Ohwada, K. Ishii, T. Inami, K. Kakurai, Y. Murakami, K. Yoshii, S. Mori, Y. Horibe, and H. Kitô, Ferroelectricity from iron valence ordering in the charge-frustrated system $LuFe_2O_4$, Nature (London) **436**, 1136 (2005).

[92] M. Naka and S. Ishihara, Electronic ferroelectricity in a dimer Mott insulator, J. Phys. Soc. Jpn. **79**, 063707 (2010).

[93] C. Hotta, Quantum electric dipoles in spin-liquid dimer Mott insulator κ-$ET_2Cu_2(CN)_3$, Phys. Rev. B **82**, 241104(R) (2010).

[94] P. Pfeuty, The one-dimensional Ising model with a transverse field, Ann. Phys. **57**, 79 (1970).

[95] A. Ono, S. Okumura, S. Imai, and Y. Akagi, High harmonic generation from electrons moving in topological spin textures, Phys. Rev. B **110**, 125111 (2024).

[96] J.-M. Liu, *Nonlinear Photonics* (Cambridge University Press, Cambridge, England, 2022)

[97] A. Ono, Extracting nonlinear dynamical response functions from time evolution, Phys. Rev. Lett. **135**, 026401 (2025).